IEEE Access
Multidisciplinary ⋮ Rapid Review ⋮ Open Access Journal

Received 18 April 2024, accepted 13 May 2024, date of publication 21 May 2024, date of current version 6 June 2024.

Digital Object Identifier 10.1109/ACCESS.2024.3403725

RESEARCH ARTICLE

Multi-Dimensional Sigma Shift Matrix (*nD*-SSM) Code With Adaptable Transmitter-Receiver Architecture to Support Multiclass Users for SAC-OCDMA System

HASSAN YOUSIF AHMED[1], MEDIEN ZEGHID[1,2], MAISARA MOHYELDIN GASIM[3], AND SOMIA A. ABD EL-MOTTALEB[4]

[1]Department of Electrical Engineering, College of Engineering in Wadi Alddawasir, Prince Sattam Bin Abdulaziz University, Wadi Alddawasir 11991, Saudi Arabia
[2]Electronics and Micro-Electronics Laboratory (E. μ. E. L), Faculty of Sciences, University of Monastir, Monastir 5000, Tunisia
[3]Mechanical Engineering Department, College of Engineering in Wadi Alddawasir, Prince Sattam Bin Abdulaziz University, Wadi Alddawasir 11991, Saudi Arabia
[4]Department of Mechatronics Engineering, Alexandria Higher Institute of Engineering and Technology, Alexandria 21311, Egypt

Corresponding author: Maisara Mohyeldin Gasim (mm.mohamed@psau.edu.sa)

This work was supported by Prince Sattam bin Abdulaziz University under Project PSAU/2023/01/25208.

ABSTRACT This work introduces an n-D algorithm to generate multi-dimensional Sigma Shift Matrix (nD-SSM) code sequences is proposed, which is based on spectral/temporal/spatial incoherent optical code division multiple access (OCDMA) system. Our proposed system is capable of generating code in accordance with the value of n, where $n = 1$, 2 and 3 for 1D, 2D, and 3D respectively. The nD-SSM codes improve system cardinality by eliminating multiple access interference and its accompanied phase induced intensity noise (PIIN). Additionally, the nD-SSM technique permits various users with different dimensions of codewords to send their data. The data will be sent with the lowest probability of interference. The design of transmitter-receiver structure of nD-SSM OCDMA system is described. Gaussian approximation is used to analyze performance of the proposed nD-SSM OCDMA system by investigating signal to noise ratio (SNR) and bit error rate (BER) under different conditions of transmission. The maximum allowable number of users with BER ∼10-9 is 43, 108, 140, 158 and 600, respectively for 1D-SSM, 2D-SSM, 2D-DEU, 3D-PD and 3D-SSM codes, respectively at 622 Mbps. These numbers of users with the same value of BER decreased to 18 for 1D-SSM, 46 for 2D-SSM, 2 for 2D-DEU, 82 for 3D-PD, and 237 for 3D-SSM at 2.5 Gbps. At 10 Gbps, the maximum allowable number of users are 9, 24, 40, and 97 for 1D-SSM, 2D-SSM, 3D-PD, and 3D-SSM, respectively. Accordingly, the proposed 3D-SSM code supports the larger number of users at different data rates when compared to other codes.

INDEX TERMS BER, P_{sr}, nDSSM, OCDMA, QoS, PIIN.

I. INTRODUCTION

Multiplexing techniques like wavelength division multiplexing access (WDMA) and time domain multiplexing access (TDMA) and optical code division multiplexing (OCDMA) recently become essential in the field of optical communication systems due to their ability of allowing multiple users access the same channel [1], [2], [3]. As in TDMA, users use time slots to transmit their data while in WDMA, wavelengths are used, therefore, a need for time management and large optical bandwidth is required for transmitting large data [4], [5], [6]. So, OCDMA is preferred to be used for allowing large number of users to transmit their information asynchronous without needing time management or large bandwidth due to its optical domain that make every user sends its information using unique code [7], [8], [9].

The associate editor coordinating the review of this manuscript and approving it for publication was Jonathan Rodriguez.

© 2024 The Authors. This work is licensed under a Creative Commons Attribution-NonCommercial-NoDerivatives 4.0 License.
For more information, see https://creativecommons.org/licenses/by-nc-nd/4.0/

Although OCDMA has many advantages like security and improving quality of service, it has drawback that is multiple access interference (MAI) due to cross correlation (λ_c) property of OCDMA codes that affects the system performance [10]. Spectral amplitude coding (SAC) can be used with OCDMA for eliminating MAI through using suitable detection technique [11]. In SAC-OCDMA, several codes that have different dimensions as one dimension (1)-D), two dimension (2)-D) and three dimension (3)-D) are introduced. In 1-D codes as modified double weight (MDW) [12], dynamic cyclic shift (DCS) [13], diagonal Eigen unity (DEU) [14] and multi diagonal (MD) [15], the code length, L, are linked directly to number of users, K, that leads to degradation in multiplexing capacity.

For solving the problem of capacity and length L, researchers suggested 2-D codes and that through combining any two parameters together of these parameters that are spectral, spatial, time and polarization [16]. However, increasing the capacity of 2-D leads to increasing either temporal length or spatial according to code construction that causes increasing slot duration or spatial components. As a result, this increase cause performance degradation and requires large number of encoding and decoding components which make it complex [16]. So, researchers, recently propose 3-D codes in order to reduce L and make it easy implemented and applicable [16].

In this paper, an n-D algorithm to generate multi-dimensional Sigma Shift Matrix (*nD*-SSM) code is designed and developed to give diversity in dimension selection aiming to improve system's performance of OCDMA scheme. It also uses mathematical expression that condenses traditional steps of building code in multi-dimensional in one algorithm. The proposed model for calculating the error rate is based on deriving a mathematical equation that takes into account the effect of user interference, thermal noise, and shot noise. After that we will analyze and compare the system's performance with other systems. Comparing the analytical results of the proposal with the publication demonstrated the superiority of our proposed system in accommodating the largest number of users with a high rate of data transfer, in addition to the flexibility in choosing the first, second, or third dimension.

This paper deals with the following findings:

1. Development of n-DSSM algorithm.
2. Development of Multiplex to make the selection of dimensions.
3. Simulation validation of *n*-D code analytical model.
4. Proposal of configurable transceiver structure.
5. Accommodation of large number of simultaneous users with high bit rate.

The rest of this paper will be organized as follows. Section II gives an idea about related works that crosses with our proposal. Section III explains how the code is built, its characteristics, and the three dimensions on which it is built (Spectral/Temporal/Spatial). Section IV presents the sender and receiver architecture of the proposed system. Analyzing the system performance by providing the necessary equations will be presented in Section V. The results of numerical analysis and simulation are presented in Section VI. Finally, the conclusions are drawn in Section VII.

II. RELATED WORKS

In [12], the authors proposed 1-D MDW code with SAC-OCDMA system, the performance of the system is studied and compared with other codes. Although, the results show improvement in performance that is related to bit error rate (BER) and K, but for large number of K, the performance of system will degrade due to presence of phase induced intensity noise (PIIN) that cause MAI. In [13], the authors proposed 1-D DCS code with SAC-OCDMA system. The obtained results show that the system can support large number of users at any code weight. In [14], the authors proposed 1-D DEU code with SAC-OCDMA system. Although, the results show good performance when compared with other codes like DCS and MD, but the code property that is non zero cross correlation leads to presence of MAI which limits the number of simultaneous users. In [15], the authors proposed 1-D MD code with SAC-OCDMA code. The performance of this code shows better performance in terms of BER and signal to noise ratio (SNR) when compared with other codes like random diagonal (RD) but this code has zero cross correlation which may be difficult to implement practical. In [17], the authors proposed 2-D DCS code with SAC-OCDMA code. The results show short code length compared to 1-D DCS but the complexity increase due to the need of presence two photo detectors (PD) at the receiver for MAI elimination. In [18], the authors proposed 2-D DEU code with SAC-OCDMA code. The results show short code length compared to 1-D DEU but the complexity increase due to the need of presence two photo detectors (PD) at the receiver for MAI elimination. In [19], [20], [21], [22], [23], [24], [25], the authors proposed 2-D MD code with SAC-OCDMA code. Although, the system can support large number of users compared to 1-D MD code but narrow filters are required at the receiver for detecting the signal. In [20], the authors proposed 3-D hybrid code between perfect difference code (PD) and MD code based on 2D-PD code and 1-D MD code. The suggested 3-D PD/MD code also require two PD at receiver which make the system implementation more complex. In [26], the authors introduced a 2D OCDMA code by extending the successive weight (SW) code. They combined this code with orthogonal frequency division multiplexing (OFDM) to create a 2D spectral/spatial OCDMA code. While the results demonstrated that the proposed system achieved higher transmission capacity, it required long code lengths, which in turn necessitated a large number of encoding and decoding components. In [27], the authors investigated the use of a 2D cyclic shift (CS) code in a spectral/time encoding scheme. This code is notable for its zero cross-correlation (ZCC) property, which mitigates the effects of MAI and reduces the impact of PIIN. In [17], the authors explored

the utilization of 2D permutation vectors (PV) in OCDMA systems to implement a spectral/spatial code. This approach aimed to reduce MAI and enhance the optical system's cardinality. In [28], the authors proposed a 3D OCDMA code that employed a 1D MD code for the spatial domain and a 1D DEU for spectral and temporal spreading. This system required higher cardinality to achieve higher data rates. In [29], a 3D OCDMA code based on a spectral, temporal, and spatial single-weight ZCC was proposed. The results indicated that a total code length of 273 was necessary to accommodate 454 users, making the implementation of this code more complex.

III. DESCRIPTION OF MULTI-DIMENSIONAL SSM SYSTEM

This paper proposes an *n*D coding scheme for SAC family called $nD-SSM$ code. $nD-SSM$ (Sigma Shift Matrix) code is characterized by four basic performance parameters including n, Tl, λc and w_i. Where n is the dimension level ($1 <= n <= 3$), Tl represents the total code length, λc is the cross-correlation and w_i is the code weight for OCDMA domains (spectral; time; spatial). To overcome the limits of one domain OCDMA code, *n*D encoding approaches have been developed by combining OCDMA domains. Therefore, in the $nD-SSM$ code, "i" is the dimension index and "i" is ranging between 1 and n. $nD-SSM$, can be expressed as

$$nD-SSM=\prod_{i=1}^{n}(\mathrm{C}_i)_{k_i\times r_i} \tag{1}$$

where C_i represents the matrix of generated code sequences. C_i is $k_i \times r_i$ matrix, where k_i represents the number of users for i-dimension and r_i is the length in code matrix respectively. For instance, the design of 3D-SSM codes needs three 1D-SSM matrix: $\mathrm{C}_1, \mathrm{C}_2, \mathrm{C}_3$ for encoding the spectral, temporal, and spatial components, respectively. Moreover, the $nD-SSM$ codes are generated to satisfy the following properties:

Properties	$nD-SSM$ codes
λ_c	=1
w_i	$\in \{w_1, w_2, w_3\}$
r_i	$(k_i(w_i-1)+1)$
k	$\prod_{i=1}^{n} k_i$
Tl	$\prod_{i=1}^{n} r_i$

The construction of 1D SSM is given in section A.

A. CONSTRUCTION OF 1D SSM CODE

The 1D-SSM code is a combination of (w-2) shift (Us) matrices and one identity (I) matrix, as given in below equation and its code length is calculated by: $r = K(w-1)+1$.

$$1D-SSM=f(I,Us)=\left\{I+\sum_{m=0}^{W-2}Us_{i+m,j}\right\}_{K\times r} \tag{2}$$

The following steps summarize the construction process for four users as example.

Step 1: construction of Shift Matrix

Reference to the concepts of algebra and operator theory, let H be a separable Hilbert space. The shift operator $S: H \longrightarrow H$ defined by $Se_n = e_{n+1}$ for $n = 0, 1, 2, 3, \ldots$ with respect to the orthonormal basis $\{e_n\}_{n=0}^{\infty}$ of H has a matrix representation written as

$$Us=\begin{bmatrix} 0 & 1 & 0 & \cdots & 0 \\ 0 & 0 & 1 & \ldots & \square \\ 0 & 0 & 0 & \ddots & \square \\ 0 & 0 & 0 & \ddots & \square \\ \vdots & \vdots & \vdots & \cdots & 1 \\ 0 & 0 & 0 & \ldots & 0 \end{bmatrix} \tag{3}$$

Us is an upper shift matrix with "1s" only on the successive super diagonal and "0s" elsewhere. Moreover, Us is designed with a $K \times r$ diagonal matrix, where K rows give the number of subscribers and r columns represent the length of Us code sequences respectively. Additionally, the $(i+m, j)$:th component of Us for i =0,....K-1 and j =0,....r-1, in SSM code sequence is designed such that:

$$Us_{i+m,j}=\delta_{i(w-1)+1+m,j} \tag{4}$$

where $\delta_{i,j}$ is the Kronecker delta symbol and $m \in [0, w-2]$. In the design of Us, w is used to define the position of "1s" in each row. This arrangement leads to a cross correlation between subsequent and any rows of $Us_{i+m,j}$ matrix equal to 0. Thus, for 4 subscribers ($K = 4$), with $w = 4$, three shift matrices $Us_{i+m,j}$ will be generated as follows

$$Us_{i,j}=\begin{bmatrix} 01000000000000 \\ 00001000000000 \\ 00000001000000 \\ 00000000001000 \end{bmatrix};\ \text{for } m=0$$

$$Us_{i+1,j}=\begin{bmatrix} 00100000000000 \\ 00000100000000 \\ 00000000100000 \\ 00000000000100 \end{bmatrix};\ \text{for } m=1$$

$$Us_{i+2,j}=\begin{bmatrix} 00010000000000 \\ 00000010000000 \\ 00000000010000 \\ 00000000000010 \end{bmatrix};\ \text{for } m=2$$

Step 2: Construction of Identity Matrix

In the SSM code matrix, the identity matrix is designed with a $K \times r$ diagonal matrix, denoted by $I_{K\times r}$ with entries equal to the Kroncker delta.

$$\delta_{i,j}=\begin{cases} 0 & \text{if } i \neq j \\ 1 & \text{if } i=j \end{cases} \tag{5}$$

where $i = 0, 2, 3, \ldots, K-1$ and $j = 0, 2, 3, \ldots, r-1$.

Step 3: Construction of SSM code matrix:

Using the above-mentioned properties and Eq. (1), *SSM* code for 4 subscribers and with w = 4 can be written as:

$$SSM - 1D = I + Us_{i,j} + Us_{i+1,j} + Us_{i+2,j} \tag{6}$$

to conclude $\lfloor SSM \rfloor_{4\times4}$ can be written as

$$SSM = \begin{bmatrix} 1111000000000 \\ 0100111000000 \\ 0010000111000 \\ 0001000000111 \end{bmatrix}_{4\times13} \tag{7}$$

B. CONSTRUCTION OF 2D AND 3D SSM CODES

The 2D-SSM code sequences are designed from the extension of the 1D-SSM in both spectral and spatial domains. Hence, for spectral C_1 is used and for spatial C_2 is used to generate the 2D-SSM code and is expressed as follows:

$$A_{q,x} = {C_{1,q}}^T \times C_{2,x} \tag{8}$$

where q =1,2,... K_1, and x =1,2,..., K_2. Therefore, the total code *Tl* length and system capacity *K* (number of users) are $T_l = r_1 r_2$ and $k = K_1 \cdot K_2$, respectively. Likewise for the 3D-SSM, it requires three code sequences C_1, C_2, and C_3, where C_1 encodes the spectral element; the C_2 encodes the temporal component; and the C_3 encodes the spatial co. The 3D-SSM code expression is $A_{q,x,y} = C^T_{1,q} \times C_{2,x} \times C_{3,y}$. An example of the 3D code sequence is presented in Table 1 for ((K_i, w_i) =(2,3)). Moreover, the 2D- SSM code development using two 1D-SSM code sequences $(C_{1,i}, C_{2,j})$, is also highlighted in purple in Table 1.

C. *nD*–SSM CODE PROPERTIES

To express the cross-correlation of the *nD* –SSM code, based on C_i and its complementary ,2^n (A^d) characteristic matrices where $d = 1,..,2^n$ are defined. For instance for 3D-SSM code, the elements of the eight decoding correlation functions at the receiver end for each PD are defined as:

$$A^d = \begin{cases} A^1 = C_1^T \times C_2 \times C_3 \\ A^2 = \overline{C_1}^T \times C_2 \times C_3 \\ A^3 = C_1^T \times \overline{C_2} \times C_3 \\ A^4 = \overline{C_1}^T \times \overline{C_2} \times C_3 \end{cases} \quad and$$

$$\times \begin{cases} A^5 = {C_1}^T \times C_2 \times \overline{C_3} \\ A^6 = \overline{C_1}^T \times C_2 \times \overline{C_3} \\ A^7 = C_1^T \times \overline{C_2} \times \overline{C_3} \\ A^8 = \overline{C_1}^T \times \overline{C_2} \times \overline{C_3} \end{cases} \tag{9}$$

Similarly, for 2d-SSM, only four matrices A^1, A^2, A^3, and A^4 are defined based on C_1, $\overline{C_1}$, C_2, $\overline{C_2}$ as marked in purple in equation 7.

Therefore, the cross-correlation R^d between A^d and A can be written as:

TABLE 1. 2D and 3D SSM code sets.

	$C_{2,0}$=[11100], $C_{3,0}$=[10011]
${C_{1,0}}^T = \begin{bmatrix}1\\1\\1\\0\\0\end{bmatrix}$	$U_{0,0,0} \begin{bmatrix}11100\\11100\\11100\\00000\\00000\end{bmatrix} \begin{bmatrix}00000\\00000\\00000\\00000\\00000\end{bmatrix} \begin{bmatrix}00000\\00000\\00000\\00000\\00000\end{bmatrix} \begin{bmatrix}11100\\11100\\11100\\00000\\00000\end{bmatrix} \begin{bmatrix}11100\\11100\\11100\\00000\\00000\end{bmatrix}$
${C_{1,1}}^T = \begin{bmatrix}0\\0\\1\\1\\1\end{bmatrix}$	$U_{1,0,0} \begin{bmatrix}00000\\00000\\11100\\11100\\11100\end{bmatrix} \begin{bmatrix}00000\\00000\\00000\\00000\\00000\end{bmatrix} \begin{bmatrix}00000\\00000\\00000\\00000\\00000\end{bmatrix} \begin{bmatrix}00000\\00000\\11100\\11100\\11100\end{bmatrix} \begin{bmatrix}00000\\00000\\11100\\11100\\11100\end{bmatrix}$
	$C_{2,1}$=[01011], $C_{3,0}$= [10011]
${C_{1,0}}^T = \begin{bmatrix}1\\1\\1\\0\\0\end{bmatrix}$	$U_{0,1,0} \begin{bmatrix}01011\\01011\\01011\\00000\\00000\end{bmatrix} \begin{bmatrix}00000\\00000\\00000\\00000\\00000\end{bmatrix} \begin{bmatrix}00000\\00000\\00000\\00000\\00000\end{bmatrix} \begin{bmatrix}01011\\01011\\01011\\00000\\00000\end{bmatrix} \begin{bmatrix}01011\\01011\\01011\\00000\\00000\end{bmatrix}$
${C_{1,1}}^T = \begin{bmatrix}0\\0\\1\\1\\1\end{bmatrix}$	$U_{1,1,0} \begin{bmatrix}00000\\00000\\01011\\01011\\01011\end{bmatrix} \begin{bmatrix}00000\\00000\\00000\\00000\\00000\end{bmatrix} \begin{bmatrix}00000\\00000\\00000\\00000\\00000\end{bmatrix} \begin{bmatrix}00000\\00000\\01011\\01011\\01011\end{bmatrix} \begin{bmatrix}00000\\00000\\01011\\01011\\01011\end{bmatrix}$
	$C_{2,0}$=[11100], $C_{3,1}$= [01110]
${C_{1,0}}^T = \begin{bmatrix}1\\1\\1\\0\\0\end{bmatrix}$	$U_{0,0,1} \begin{bmatrix}00000\\00000\\00000\\00000\\00000\end{bmatrix} \begin{bmatrix}11100\\11100\\11100\\00000\\00000\end{bmatrix} \begin{bmatrix}11100\\11100\\11100\\00000\\00000\end{bmatrix} \begin{bmatrix}11100\\11100\\11100\\00000\\00000\end{bmatrix} \begin{bmatrix}00000\\00000\\00000\\00000\\00000\end{bmatrix}$
${C_{1,1}}^T = \begin{bmatrix}0\\0\\1\\1\\1\end{bmatrix}$	$U_{1,0,1} \begin{bmatrix}00000\\00000\\00000\\00000\\00000\end{bmatrix} \begin{bmatrix}00000\\00000\\11100\\11100\\11100\end{bmatrix} \begin{bmatrix}00000\\00000\\00000\\00000\\00000\end{bmatrix} \begin{bmatrix}00000\\00000\\11100\\11100\\11100\end{bmatrix} \begin{bmatrix}00000\\00000\\00000\\00000\\00000\end{bmatrix}$
	$C_{2,1}$=[01011], $C_{3,1}$= [01110]
${C_{1,0}}^T = \begin{bmatrix}1\\1\\1\\0\\0\end{bmatrix}$	$U_{0,1,1} \begin{bmatrix}00000\\00000\\00000\\00000\\00000\end{bmatrix} \begin{bmatrix}01011\\01011\\01011\\00000\\00000\end{bmatrix} \begin{bmatrix}01011\\01011\\01011\\00000\\00000\end{bmatrix} \begin{bmatrix}01011\\01011\\01011\\00000\\00000\end{bmatrix} \begin{bmatrix}00000\\00000\\00000\\00000\\00000\end{bmatrix}$
${C_{1,1}}^T = \begin{bmatrix}0\\0\\1\\1\\1\end{bmatrix}$	$U_{1,1,1} \begin{bmatrix}00000\\00000\\00000\\00000\\00000\end{bmatrix} \begin{bmatrix}00000\\00000\\01011\\01011\\01011\end{bmatrix} \begin{bmatrix}00000\\00000\\01011\\01011\\01011\end{bmatrix} \begin{bmatrix}00000\\00000\\01011\\01011\\01011\end{bmatrix} \begin{bmatrix}00000\\00000\\00000\\00000\\00000\end{bmatrix}$

Case of 2D-SSM:

$$R^d_{q,x} = \sum_{i=1}^{r1} \sum_{j=1}^{r2} a^d_{i,j} a_{i+q,j+x} \tag{10-a}$$

where $a^d_{i,j,d}$ (or $a^d_{i,j}$), and $a_{i+q,j+x,d+y}$ (or $a_{i+q,j+x}$) denote the elements of A^d and $A_{q,x}$, respectively.

Case of 3D-SSM:

$$R^d_{q,x,y} = \sum_{i=1}^{r_1} \sum_{j=1}^{r_2} \sum_{d=1}^{r} a^d_{i,j,d} a_{i+q,j+x,d+y} \tag{10-b}$$

Further, Table 2 shows the results of the cross-correlation of the 3D SSM code according to the characteristic matrices A^d. We can also see from Table 2 that $R^{(0)}$, $R^{(2)}$, $R^{(5)}$, and $R^{(7)}$ when (q, x, y) =(0, x, 0) and (q, x, y) = ($\neq$0,x, $\neq$0) reflect the cross-correlation of the SSM code in 2D.

D. *nD*-SSM PSEUDO ALGORITHM

nD-SSM coding algorithm is derived by using *n* C_i matrices. The process of constructing the proposed code is summarized

TABLE 2. Lists the correlation properties of the 2-D and 3-D codes for each PD.

	$R^{(0)}(q,r,s)$	$R^{(1)}(q,r,s)$	$R^{(2)}(q,r,s)$	$R^{(3)}(q,r,s)$	$R^{(4)}(q,r,s)$	$R^{(5)}(q,r,s)$	$R^{(6)}(q,r,s)$	$R^{(7)}(q,r,s)$
$q=0, r=0, s=0$	$w_1w_2w_3$	0	0	0	0	0	0	0
$q=0, r\neq 0, s=0$	w_1w_3	0	$w_1(w_2-1)w_3$	0	0	0	0	0
$q\neq 0, r=0, s=0$	w_2w_3	0	0	w_2w_3	0	0	0	0
$q\neq 0, r\neq 0, s=0$	w_3	0	$w_3(w_2-1)$	w_3	0	0	$(w_3-1)(w_2-1)$	0
$q=0, r=0, s\neq 0$	w_1w_2	$w_1w_2(w_3-1)$	0	0	0	0	0	0
$q=0, r\neq 0, s\neq 0$	w_1	$w_1(w_3-1)$	$w_1(w_2-1)$	0	$w_1(w_2-1)(w_3-1)$	0	0	0
$q\neq 0, r=0, s\neq 0$	w_2	$w_2(w_3-1)$	0	w_2	0	$w_2(w_3-1)$	0	0
$q\neq 0, r\neq 0, s\neq 0$	1	w_3-1	w_2-1	1	$(w_2-1)(w_3-1)$	w_3-1	w_2-1	$(w_2-1)(w_3-1)$

in the algorithm 1. Algorithm 1 has 3 stated inputs: n, and set numbers of k_i and w_i. The proposed design of *nD*-SSM coding technique includes 3 steps to determine the $n\mathrm{C}_i$ matrices:

- Forming total code length per dimension. (line 3)
- Generating C_i matrix (line 4 to line 5).
- Merging the generated C_i matrices into $nD-SSM$ (line 7-line 10).

Proposed n-Dimensional Sigma Shift Matrix code

Input : $K_i = \{K_1, K_2, K_3\}$
Input : $w_i = \{w_1, w_2, w_3\}$
Input : n
Output : $nD-SSM$ // matrix code
1. Define $K=0$; $r_i = 0//K$ is the total number of users and r_i is the total code length per dimension
2. *For* $i = 1$ *to* n
3. $r_i = k_i\,(w_i-1)+1$
4. for $j = 0$ to $k_i - 1$
   4.1. $\mathrm{C}_{i_j}\,((r_i-1)$ downto $0) = (\ others =>' 0')$; // C_{i_j} is the j row in the C_i matrix
   4.2. $\mathrm{C}_{i_j}\,(r_i-2-j\,(w_i-1)$ *downto* $r_i+j-w_i(j+1)) = (\ others =>' 1\ ')$;
   4.3. If j $= 0'$
      4.3.1. $\mathrm{C}_{i_j}\,(r_i-1) =' 1'$;
      Else
      4.3.2. $\mathrm{C}_{i_j}\,((r_i-j)-1) =' 1'$;
   4.4. End if;
5. Endfor
6. Endfor
7. If n = 1
   7.1. Return $nD-SSM = \mathrm{C}_1$
8. Elsif n = 2
   8.1. Return $nD-SSM = \mathrm{C}_1{}^T \times \mathrm{C}_2$
9. Else
   9.1. Return $nD-SSM = \mathrm{C}_1{}^T \times \mathrm{C}_2 \times \mathrm{C}_3$
10. endif

IV. n-D-SSM TRANSMITTER-RECEIVER ARCHITECTURE

A. DESIGN OF 3D-SSM SYSTEM

For the sake of clarity, let us assume that $\boldsymbol{r_1}$ is equal to M, $\boldsymbol{r_2}$ is equal to N and $\boldsymbol{r_3}$ = P. Figure 1 is a schematic representation of a spectral/temporal/spatial OCDMA network that incorporates star couplers, MNP transmitter-receiver pairs, and other related components. Users of *MNP* combination can be supported by the system. All transmitter-receiver pairs are designated with a 3D-SSM codewords $\boldsymbol{a_{g,h,l}}$, $g = 0,1,2,3,\ldots M\text{-}1$, $h = 0,1,2,3,\ldots N\text{-}1$, $l = 0,1,2,3,\ldots P\text{-}1$. The transmitter initially encodes the binary data it receives by associating each data with its matching codeword. Subsequently, the transmitter transmits the encoded data codewords to the receivers through the star couplers.

The receiver incorporates a double balanced detection system consisting of eight photodiodes, which collects the intended spectra and converts it into a corresponding codeword.

B. DESIGN OF 3D-SSM TRANSMITTER PART

The transmitter comprises the data source, optical source, Mach-Zehnder modulator (MZM), fiber Bragg gratings (FBGs) delay lines, splitter, and a series of star couplers (SCs). Firstly, the external modulator MZM converts each user data into an optical pulse using an optical source, and then the modulated data are sent to FBGs to perform spectral coding relying on the spectral pattern $\mathrm{X_g}$ of SSM code, where wavelengths matched with "1" are spectrally encoded whereas other do not matched with "1" are reflected and filtered out. Secondly, output of FBGs are fed into delay line to carry out temporal coding according to the SSM code's $\mathrm{Y_h}$ sequence. Thirdly, the spectrally and temporally coded pulses are delivered to SCs for spatial coding in accordance with SSM code's $\mathrm{Z_l}$ sequence. Hence, each user's data is coded spectrally, temporally, and spatially according to the 3D-SSM code. The 3D SSM OCDMA system is implemented using a combination of M × N × P transmitter and receiver modules. Each pair of modules utilizes the $\boldsymbol{E_{g,h,l}}$3D-SSM codeword. The interface between the transmitter-receiver pairs is established by star couplers, which have $N \times P$ inputs and outputs.

C. DESIGN OF 3D-SSM RECEIVER PART

The structure of the receiver for 3D-SSM OCDMA scheme is explained in Fig. 3, which encompasses several switches connected to optical combiners, four balanced detectors, and an integrator to carry out the required decision. The combiners are used to cumulative optical signal outputs from star couplers that correspond to Z_l or the complementary code sequence $\bar{Z}_l$. The four correlators associated with Y_h and $\bar{Y}_h$ are constructed using optical delay lines. Two correlators, correlators 1 and 3, are connected to Y_h using w_2 optical delay lines. On the other hand, correlators 2 and 4 are connected to $\bar{Y}_h$ using $N - w_2$ optical delay lines. The balanced detectors

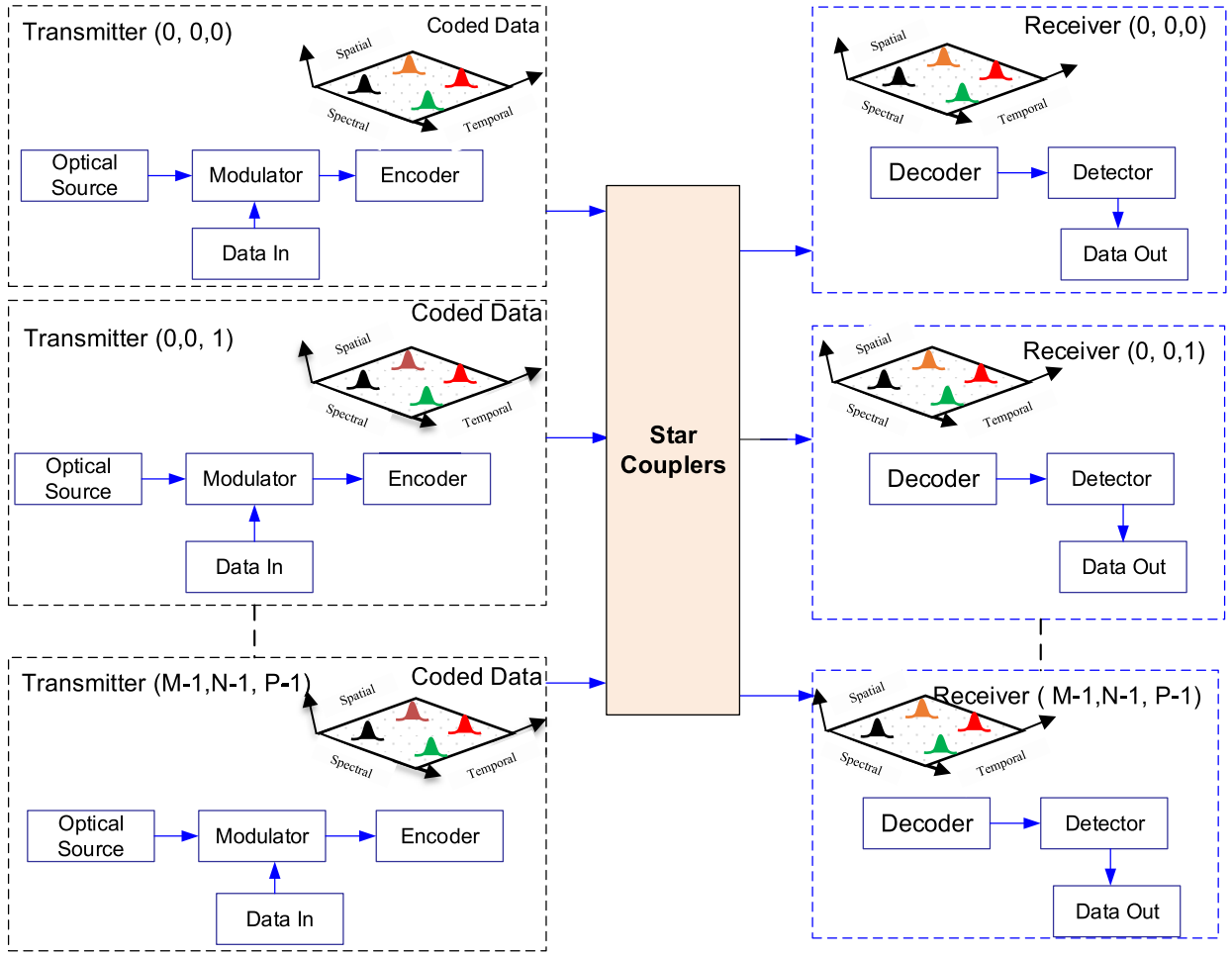

FIGURE 1. Proposed architecture of configurable transceiver 3D SSM system.

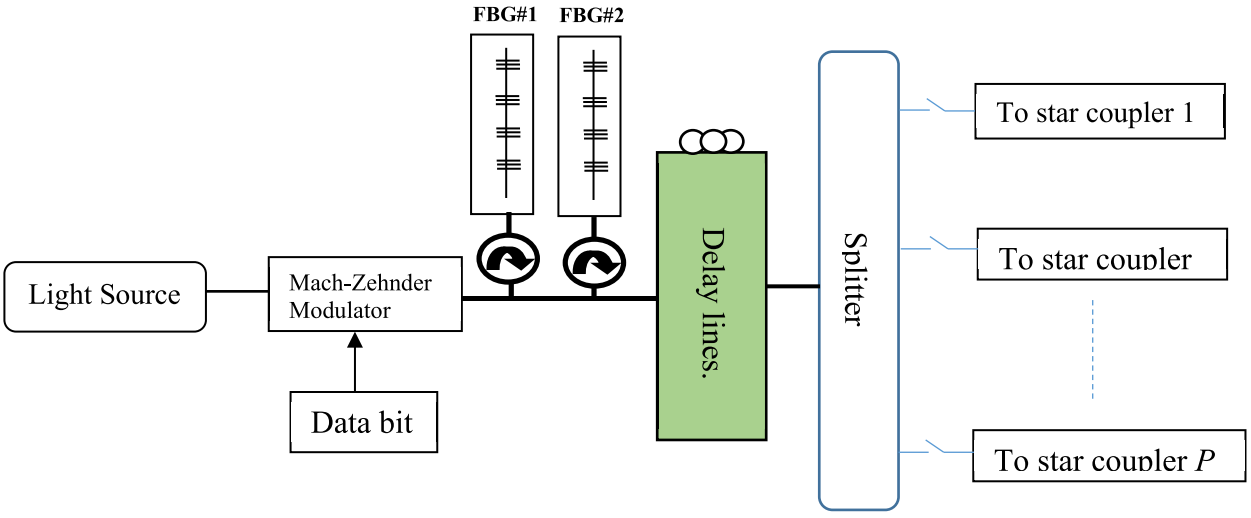

FIGURE 2. Proposed architecture of configurable transceiver 3D SSM system.

are set with dual sets of Fiber Bragg Gratings (FBGs) and two photodiodes. The FBGs 1-8 of the balanced detectors are tuned to match the spectral code sequence corresponding to X_g, and they all have an equal number of gratings.

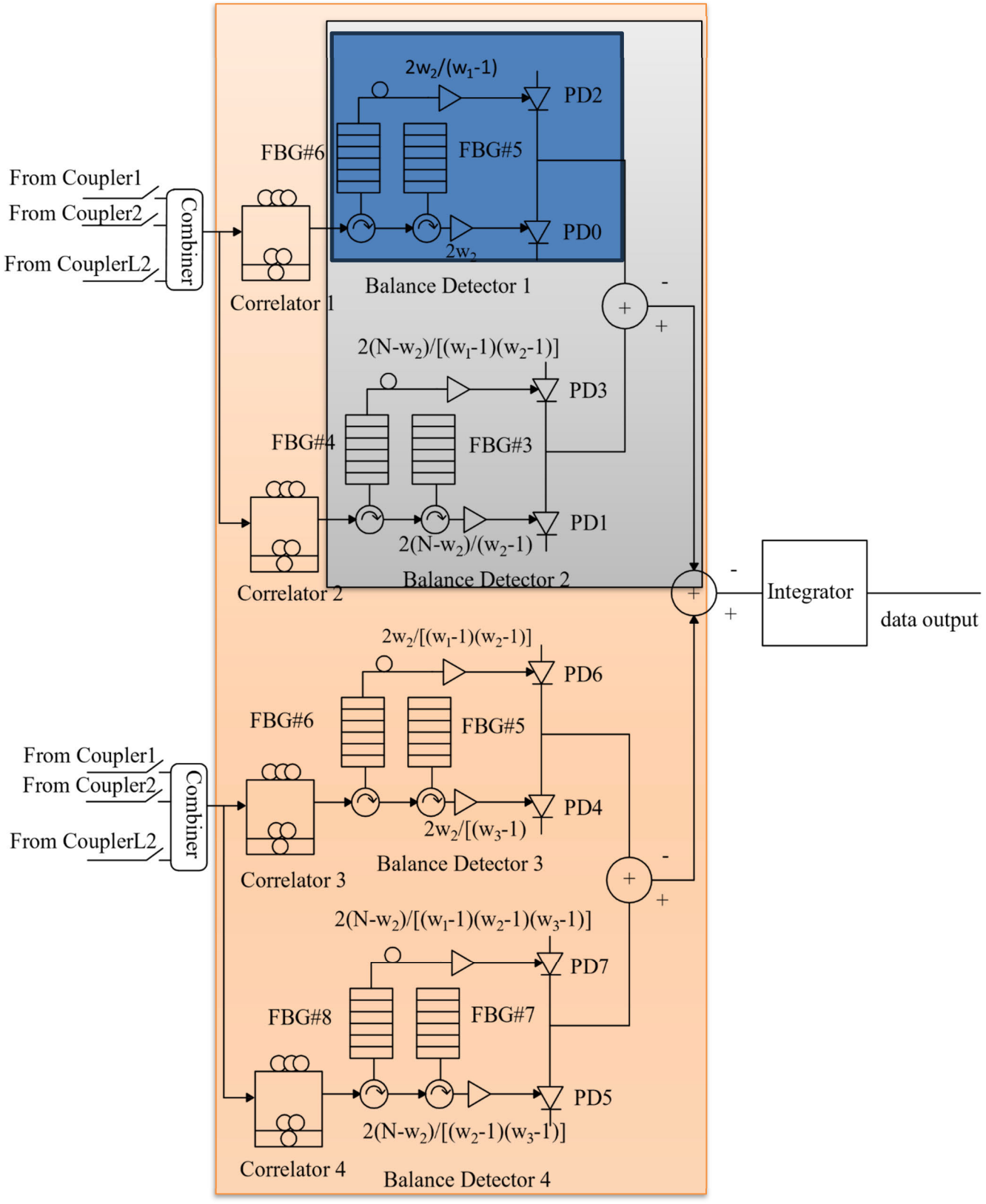

FIGURE 3. Receiver of nD-SSM OCDMA system: blue color (1D), gray color (2D) and orange color (3D).

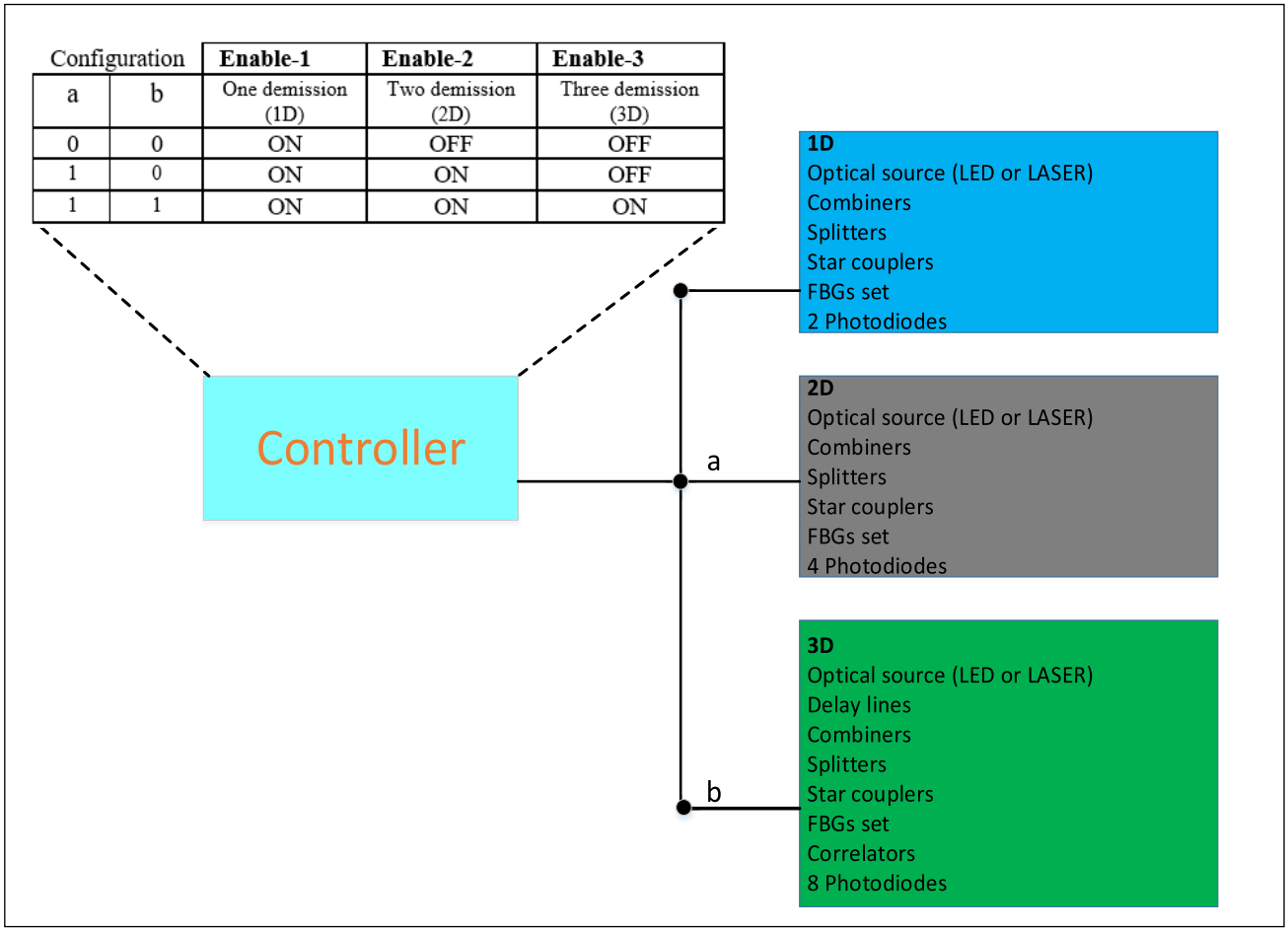

FIGURE 4. nD-SSM Transceiver structure operation.

D. PROPOSED OF ND-SSM TRANSCEIVER STRUCTURE

The main objective of this work is to develop a new algorithm to generate multi-dimensional Sigma Shift Matrix (*n*D-SSM) code sequences based on spectral/ temporal/ spatial incoherent OCDMA system. This system has the flexibility to generate the code base on selection of n value where n =1, 2 and 3 for 1D, 2D and 3D respectively. The transmitter-receiver structure should have the flexibility to select the desired dimension based on the input as given in Fig.5. The controller acts as a multiplexer (MUX) to enable and disable the portion in the entire structure that runs either 1D or 2D or 3D. Execution of the MUX is controlled by two signals a and b in which the transceiver structure is fully built based on 3D that encapsulates both 1D and 2D. 1D portion components always exist as primary case to entire structure that is why always the MUX treats it as ON state. When $a = 1$ and $b = 0$ (ON-OFF state), the selection function is performed by choosing 2D encoding mode which has a 1D encoding mode by default. When a and b =1 (ON-ON state), the selection function is performed by choosing 3D encoding mode which has a 1D and 2D encoding modes by default. In terms of hardware, most of basic components are the same except for 3D coding which requires much more, especially temporal components such as delay lines and correlators.

V. PERFORMANCE ANALYSIS

When a wide-band pulse is fed into the group of Fiber Bragg Gratings (FBGs), the non-coherent light fields are combined and directed towards a photodetector. The phase fluctuations of the fields result in an intensity fluctuation in the output of the photodetector [10], [11]. The coherence time (τc) of a thermal source is defined as in [10], [22].

$$\tau_c = \frac{\int_0^\infty G^2(v)dv}{\left[\int_0^\infty G(v)dv\right]^2} \tag{11}$$

G(v) represents the power spectral density (PSD) of the source in the single sideband. Furthermore, the variance in photocurrent resulting from the detection of a perfectly unpolarized thermal light, generated through spontaneous emission, can be expressed as:

$$\left\langle i^2 \right\rangle = \left\langle I_{PIIN}^2 \right\rangle + \left\langle I_{shot}^2 \right\rangle + \left\langle I_{thermal}^2 \right\rangle \tag{12}$$

where $\langle I_{shot}^2 \rangle$ denotes shot noise, $\langle I_{PIIN}^2 \rangle$ represents phase induced intensity noise and $\langle I_{thermal}^2 \rangle$ is the thermal noise. Thus, Eq. (12) can also be written as:

$$\left\langle i^2 \right\rangle = BI^2\tau_c + 2eIB + \frac{4k_bT_nB}{R_L} \tag{13}$$

where:

e = electron charge.
I = average photocurrent and I^2 is the PSD of I.
τ_c = coherence time of source.
B = noise-equivalent electrical bandwidth of the receiver.
K_b = Boltzmann's constant.
T_n = absolute receiver noise temperature.
R_L = receiver load resistor.

Equation No. (25) contains three basic elements, which are shot, PIIN [10], [11] and thermal noises. The combined impact of PIIN and shot noise follows a negative binomial distribution. [18]. The suggested SSM based OCDMA is subjected to a mathematical analysis under similar hypotheses as those employed in [10], [11], [12], [13], [14]:

1) Each light source is ideally un-polarized, and its spectrum is flat over the bandwidth [$\boldsymbol{v}_o$-$\Delta\boldsymbol{v}$/2, $\boldsymbol{v}_o$ + $\Delta\boldsymbol{v}$/2], where v_o is the central optical frequency and $\Delta\boldsymbol{v}$ is the optical source bandwidth in Hertz.
2) Each power spectral element possesses the same spectral width.
3) Every user possesses the same power at the recipient's end.
4) The bit stream from each user is synced individually.

In Eq. (26), the total effect of PIIN and shot noise obeys negative binomial distribution, and thermal noise has a Gaussian distribution. Therefore, Gaussian approximation is used for all *noise sources* to easily analyze the system's performance [18]. *As per Gaussian Approximation analysis, t*he power spectral density (PSD) of the received optical signals can be written as [10], [11], [12], [13], [14]:

$$r(v) = \frac{P_{sr}}{\Delta v}\sum_{f=1}^{K} d_f \sum_{i=1}^{M} C_f(i).rect(i). \tag{14}$$

$$r(v) = \frac{P_{sr}}{\Delta v}\sum_{f=1}^{K} d_f \sum_{i=1}^{M} C_f(i).rect(i) \tag{15}$$

where P_{sr} is the effective power of a broad-band source at the receiver, K is the number of active users and M is the 1D-SSM code length, $\boldsymbol{d_f}$ is the data bit of the f-th user that is "1" or "0," and *rect (i)* is the function expressed as:

$$\begin{aligned} rect(i) &= u\left[v - v_0 - \frac{\Delta v}{2r}(-M + 2i - 2)\right] \\ &\quad - u\left[v - v_0 - \frac{\Delta v}{2M}(-M + 2i - 2)\right] \\ &= u\left(\frac{\Delta v}{M}\right) \end{aligned} \tag{16}$$

TABLE 3. Model parameters values used in numerical calculations.

Parameter	Value (unit)
Data rate	622 Mbps, 2.5 Gbps, and 10 Gbps
Received power	-10 dBm
Responsivity of photodetector	0.75
Number of users	Varies from 1 to 600
Spectral codelength	3, 7, and 13
Temporal code length	3
Spatial code length	3, 7, 13, and 21
Electrical bandwidth	0.5× Temporal code length × data rate Hz
Receiver load resistance	1030 Ω
Electron charge	1.6×10^{-19} C
Receiver noise temperature	300 K
Boltzmann constant	1.38×10^{-23} J/K

where $u(v)$ is the unit step function expressed as

$$u(v) = \begin{cases} 1, & v \geq 0 \\ v0, & v < 0 \end{cases} \tag{17}$$

A. MATHEMATICAL ANALYSIS OF 1D-SSM CODE ENCODER-DECODER STRUCTURE

(18), as shown at the bottom of the next page.

B. MATHEMATICAL ANALYSIS OF 2D-SSM CODE ENCODER-DECODER STRUCTURE

First photodiode (PD_0):

$$\begin{aligned} &I_{PD_0} \\ &= \phi\int_0^{\infty} G_0(v)dv = \frac{P_{sr}}{w_2\Delta v}\sum_{n=1}^{K} d(n)\sum_{i=0}^{M-1}\sum_{j=0}^{N-1} b_{ij}^{(0)} * b_{ij}(n)dv \\ &= \frac{\phi P_{s_s}}{w_2 M}\left[w_1w_2 + w_1\frac{(K-1)(N-1)}{MN-1}\right. \\ &\quad + w_2\frac{(K-1)(M-1)}{MN-1} \\ &\quad \left. + \frac{(K-1)(M-1)(N-1)}{MN-1}\right] \end{aligned} \tag{19}$$

Second photodiode (PD_1):

$$\begin{aligned} &I_{PD_1} \\ &= \phi\int_0^{\infty} G_1(v)dv = \frac{P_{sr}}{w_2(w_1-1)\Delta v}\sum_{n=1}^{K} d(n)\sum_{i=0}^{M-1}\sum_{j=0}^{N-1} b_{ij}^{(1)} \\ &\quad * b_{ij}(n)dv \\ &= \frac{\phi P_{sr}}{w_2 M}\left[w_2(w_1-1)\frac{(K-1)(N-1)}{MN-1}\right. \\ &\quad \left. + (w_1-1)\frac{(K-1)(M-1)(N-1)}{MN-1}\right] \end{aligned} \tag{20}$$

Third photodiode (PD_2):

$$I_{PD_2} = \phi \int_0^{\infty} G_2(v)dv = \frac{P_{sr}}{(w_1-1)\,\Delta v} \sum_{n=1}^{K} d(n) \sum_{i=0}^{M-1} \sum_{j=0}^{N-1} b_{ij}^{(2)} * b_{ij}(n)dv = \frac{\phi P_{sr}}{w_2 M} \left[w_1 \frac{(K-1)(M-1)}{MN-1} + (w_1-1) \frac{(K-1)(M-1)(N-1)}{MN-1} \right] \quad (21)$$

Fourth photodiode (PD_3) (22) and (23), as shown at the bottom of the next page.

C. 5.3 MATHEMATICAL ANALYSIS OF 3D-SSM CODE ENCODER-DECODER STRUCTURE

Based on the assumptions, the PSD of the received optical signals can be written as (24)–(34), shown at the bottom of the next page.

VI. RESULTS AND DISCUSSION OF PERFORMANCE ANALYSIS

In this section, the performance of 3D-SSM code for OCDMA is analyzed in terms of maximum allowable number of users, BER, SNR, received power and output currents of photodetectors. The results are divided into five parts. The first one contains the effect of increasing number of users on system performance while the second part shows the effect of SNR of 3D-SSM code on the system performance in terms of BER as well as comparing it with other published codes as 1D-SSM, 2D-SSM, 2D-DEU and 3D-PD codes. The third and the fourth parts study the PIIN noises and output noises from different photodetectors and the effective received power. Effect of changing spectral code length and spatial code length is given in the fifth part. Table 3 shows the values of parameters used in numerical calculations.

A. BER VERSUS NUMBER OF USERS

Figure 5 reports BER versus the number of users for 3D-SSM ($M = 3$, $N = 3$, $P = 7$), 3D-PD ($M = 3$, $N = 21$, $P = 3$), 2D-DEU ($M = 63$, P =3), 2D-SSM and 1D SSM codes at different data rates (622 Mbps, 2.5 Gbps, and 10 Gbps) and received power −10 dBm. AAs the number of users increased, the Bit Error Rate (BER) also increased. However, systems that utilize 3D codes demonstrate superior performance compared to those using 2D and 1D codes. Additionally, these systems can accommodate a higher number of users.

As the number of users increased, the Bit Error Rate (BER) also increased. However, systems that utilize 3D codes demonstrate superior performance compared to those using 2D and 1D codes. Additionally, these systems can accommodate a higher number of users.

The maximum allowable number of users with BER $\sim \mathbf{10^{-9}}$ is 43, 108, 140, 158 and 600, respectively for 1D-SSM, 2D-SSM, 2D-DEU, 3D-PD and 3D-SSM codes, respectively at 622 Mbps. These numbers of users with the same value of BER decreased to 18 for 1D-SSM, 46 for 2D-SSM, 2 for 2D-DEU, 82 for 3D-PD, and 237 for 3D-SSM at 2.5 Gbps. At 10 Gbps, the maximum allowable number of users are 9, 24, 40, and 97 for 1D-SSM, 2D-SSM, 3D-PD, and 3D-SSM, respectively. Accordingly, the proposed 3D-SSM code supports the larger number of users at different data rates when compared to other codes.

B. SNR VERSUS NUMBER OF USERS

The evaluation of signal quality is performed using a significant metric called the Signal-to-Noise Ratio (SNR).

So, the effect of SNR on system performance is given in fig. 6 that shows SNR versus active number of users for different codes at 622 Mbps, 2.5 Gbps, and 10 Gbps and received power of −10 dBm. As expected, the quality of received signal at various data rates is decreased by increasing number of active users. It is observed from fig. 7 that at same SNR as an example 21 dB, the system uses 3D-SSM can support large number of active users which is 600 at 622 Mbps, 237 at 2.5 Gbps, and 97 at 10 Gbps. Additionally, at 10 Gbps, the number of users at SNR of 21 dB are 9 and 24 for 1D and 2D-SSM codes, respectively, 40 for 3D-PD code.

C. PIIN VERSUS RECEIVED POWER AND PIIN OF EACH PHOTODIODE VERSUS RECEIVED POWER

Since the PIIN is related to the MAI, so, it is important to study its effect on received power. Figure 7 shows PIIN versus effective received power at 40 simultaneous number of users for 3D-SSM and 3D-PD codes as these codes give better performance so for simplicity, we took them for comparison in this study at data rate 622 Mbps. As concluded from fig. 7, as the received power increases, the PIIN noise increases while the system uses 3D-SSM code has massive reduction of interference due to lower PIIN noise.

Figure 8 shows the PIIN of the eight photodiodes (PD0, PD1, PD2, PD3, PD4, PD5, PD6 and PD7) versus received power at 40 active users for 3D-SSM code at 622 Mbps. It is cleared that PD7 gives the less PIIN compared to other

$$SNR_{1D} = \frac{\langle I_r \rangle^2_{SSM}}{\langle I^2_{noise} \rangle_{SSM}} = \frac{\left(\Re \frac{P_{sr}}{L} W \right)^2}{eBP_{sr}\Re \left[\frac{w_1+2K-2}{M} \right] + \frac{KB\Re^2 P^2_{sr}}{2L^2 \Delta v(w_1-1)} \left[w_1 + k - 1 + \frac{k-1}{w_1-1} \right] + \frac{4K_b T_n B}{R_L}} \quad (18)$$

photodiodes which is an example $6.29\times\mathbf{10^{-6}}$ at received power -20 dBm while the first photodiode gives the highest value of PIIN that is $3.95\times\mathbf{10^{-5}}$ for the same value of effective received power.

$$I_{PD_3} = \phi \int_0^{\infty} G_3(v)dv = \frac{P_{sr}}{w_2\,(w_1-1)\,\Delta v} \sum_{n=1}^{K} d(n) \sum_{i=0}^{M-1} \sum_{j=0}^{N-1} b_{ij}^{(3)} * b_{ij}(n)dv = \frac{\phi P_{sr}}{w_2 M} \left[(w_1-1)\,\frac{(K-1)(M-1)(N-1)}{MN-1} \right] \tag{22}$$

$$\mathbf{SNR}_{2\mathrm{D}} = \frac{\left[\frac{\phi \mathbf{P}_{sr}\mathbf{w}_1}{\boldsymbol{M}}\right]^2}{\frac{\mathbf{B}_r\phi^2\mathbf{P}_{sr}^2}{\boldsymbol{M}^2\mathbf{w}_2^2\Delta v}\left[\frac{1}{\mathbf{w}_1}\left(\mathbf{I_{PD}}_0 - \mathbf{I_{PD}}_2\right)^2 + \frac{1}{(\mathbf{w}_1-1)}\left(\mathbf{I_{PD}}_3 - \mathbf{I_{PD}}_1\right)^2\right] + 2\mathbf{eB_r}\left[\mathbf{I_{PD}}_0 + \mathbf{I_{PD}}_1 + \mathbf{I_{PD}}_2 + \mathbf{I_{PD}}_3\right] + \frac{4\,\mathbf{K_b}_n\mathbf{B_r}}{\mathbf{R_L}}} \tag{23}$$

$$r(v) = \frac{P_{sr}}{w_2 w_3 \Delta v} \sum_{k=1}^{K} d(k) \sum_{l=0}^{P-1} \sum_{i=0}^{M-1} \sum_{j=0}^{N-1} a_{i,j,l}(k) F(v,i) \tag{24}$$

$$I_0 = R \int_0^{\infty} G_0(v)dv = \int_0^{\infty} \frac{RP_{sr}}{w_2 w_3 \Delta v} \times \sum_{k=1}^{K} d(k) R^0(i,j,l) F(v,i) \tag{25}$$

$$\begin{aligned} I_0 = \frac{RP_{sr}}{w_2 w_3}\,[&w_1 w_2 w_3 + \frac{w_1 w_3 (K-1)(N-1)}{MNP-1} + \frac{w_2 w_3 (K-1)(M-1)}{MNP-1} + \frac{w_3 (K-1)(M-1)(N-1)}{MNP-1} \\ &+ \frac{w_1 w_2 (K-1)(P-1)}{MNP-1} \\ &+ \frac{w_1 (K-1)(N-1)(P-1)}{MNP-1} + \frac{w_2 (K-1)(M-1)(P-1)}{MNP-1} + \frac{(K-1)(M-1)(N-1)(P-1)}{MNP-1}\Big] \end{aligned} \tag{26}$$

$$\begin{aligned} I_1 = \frac{RP_{sr}}{w_2 w_3\,(w_2-1)}\Big[&\frac{w_1 w_3 (K-1)(N-1)}{MNP-1} + \frac{w_3 (W-1)(M-1)(N-1)}{MNP-1} \\ &+ \frac{w_1 (K-1)(N-1)(P-1)}{MNP-1} + \frac{(K-1)(M-1)(N-1)(P-1)}{MNP-1}\Big] \end{aligned} \tag{27}$$

$$\begin{aligned} I_2 = \frac{RP_{sr}}{w_2 w_3\,(w_1-1)}\Big[&\frac{w_1 w_3 (K-1)(N-1)}{MNP-1} \\ &+ \frac{w_2 w_3 (K-1)(M-1)}{MNP-1} + \frac{w_3 (K-1)(M-1(N-1))}{MNP-1} \\ &+ \frac{w_2 (K-1)(M-1)(P-1)}{MNP-1} + \frac{(W-1)(M-1)(N-1)(P-1)}{MNP-1}\Big] \end{aligned} \tag{28}$$

$$I_3 = \frac{RP_{sr}}{(w_1-1)\,(w_2-1)}\left[\frac{w_3 (W-1)(M-1)(N-1)}{MNP-1} + \frac{(W-1)(M-1)(N-1)(P-1)}{MNP-1}\right] \tag{29}$$

$$\begin{aligned} I_4 = \frac{RP}{w_2 w_3\,(w_3-1)}\Big[&\frac{w_1 w_2 (W-1)(P-1)}{MNP-1} + \frac{w_1 (W-1)(N-1)(P-1)}{MNP-1} \\ &+ \frac{w_2 (W-1)(M-1)(P-1)}{MNP-1} + \frac{(K-1)(M-1)(N-1)(P-1)}{MNP-1}\Big] \end{aligned} \tag{30}$$

$$I_5 = \frac{RP_{sr}}{w_2 w_3\,(w_2-1)}\left[\frac{w_1 (K-1)(N-1)(P-1)}{MNP-1} + \frac{w_2 w_3 (K-1)(M-1)}{MNP-1}\right] \tag{31}$$

$$I_6 = \frac{RP_{sr}}{w_2 w_3\,(w_1-1)}\left[\frac{w_2 (K-1)(M-1)(P-1)}{MNP-1} + \frac{(K-1)(M-1)(N-1)(P-1)}{MNP-1}\right] \tag{32}$$

$$I_7 = \frac{RP_{sr}}{w_2 w_3\,(w_1-1)\,(w_2-1)} \times \left[\frac{(K-1)(M-1)(N-1)(P-1)}{MNP-1}\right] \tag{33}$$

$$SNR_{3D} = \frac{\left[\frac{RP_{sr}w_1}{M}\right]^2}{\frac{MB}{2\Delta v}\left[\frac{(I_0-I_1-I_4+I_5)^2}{w_1} + \frac{(I_2-I_3-I_6+I_7)^2}{w_1-1}\right] + 2eB\,[I_0+I_1+I_4+I_5+I_2+I_3+I_6+I_7] + \frac{4K_bT_nB}{R_L}} \tag{34}$$

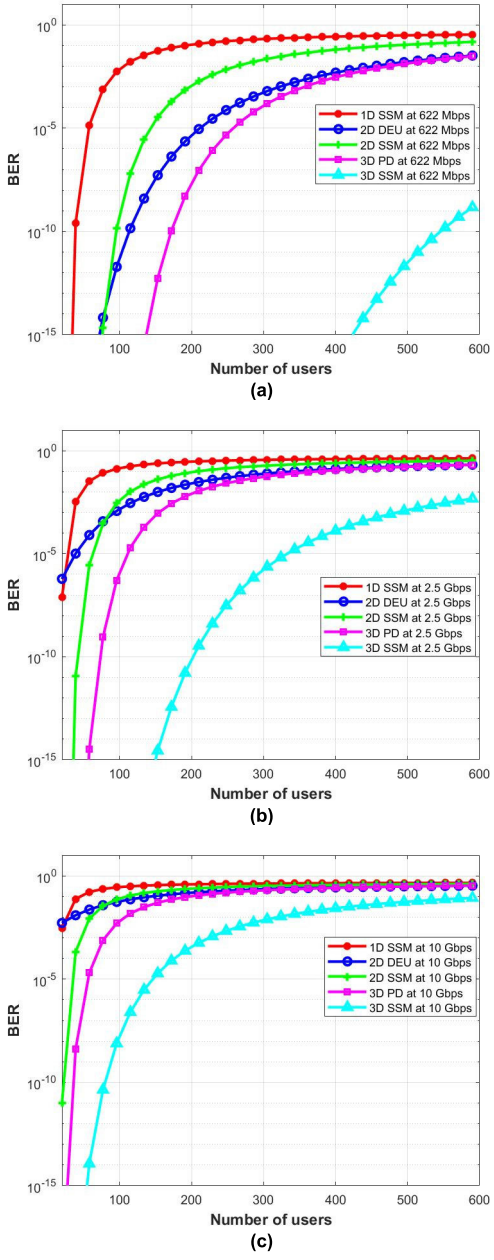

FIGURE 5. BER versus number of users for different OCDMA codes at different data rates: (a) 622 Mbps, (b) 2.5 Gbps, and (c) 10 Gbps.

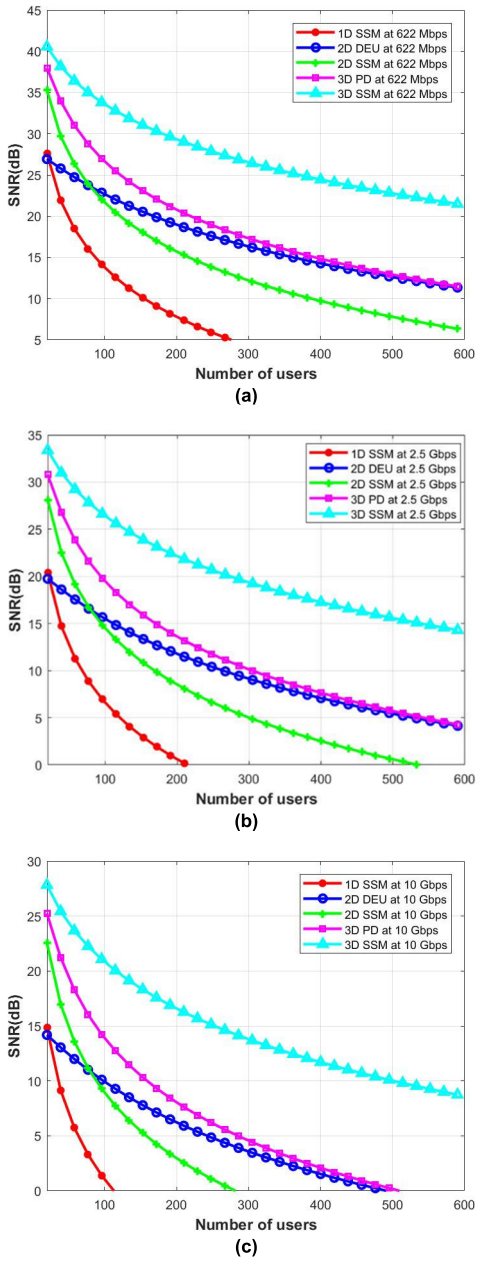

FIGURE 6. SNR versus number of users for different OCDMA codes at different data rates: (a) 622 Mbps, (b) 2.5 Gbps, and (c) 10 Gbps.

D. BER VERSUS EFFECTIVE RECEIVED POWER

Figure 9 gives BER versus received power for 1D-SSM, 2D-SSM, 2D-DEU, 3D-PD and 3D-SSM codes at 622 Mbps and 40 number of users. It is concluded from fig. 5 that, as received power increases, the BER decreases for all the codes. Also, the system uses 3D-SSM code gives the less value of BER compared to other codes. At received power = -25 dBm, the BERs values for 1D-SSM, 2D-SSM, 2D-DEU, 3D-PD and 3D-SSM codes are 0.2706, 0.2139, 0.1459, $2.909\times\mathbf{10}^{-14}$ and $9.914\times\mathbf{10}^{-16}$, respectively. So, an improvement of PIIN suppression is attained for 3D-SSM code.

E. THE EFFECT OF CHANGING THE SPECTRAL LENGTH AND THE SPATIAL LENGTH OF 3D-SSM CODE ON THE SYSTEM PERFORMANCE

Here, we discuss the relation between the system performance and the implementation complexity across various data rates and received power -10 dBm for 3D-SSM code. As shown from figs. 10 and 11, increasing the value of code spectral length M with constant value of time spreading code length N and spatial code length P leads to degradation in system performance. Also, for constant values of M and N and increasing the value of P, leads to increasing the value of BER but gives better performance and large

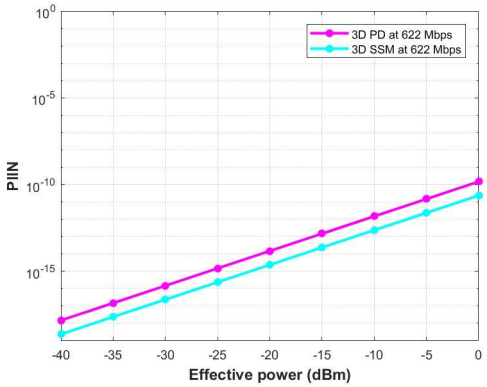

FIGURE 7. PIIN versus effective power for 3D-SSM code.

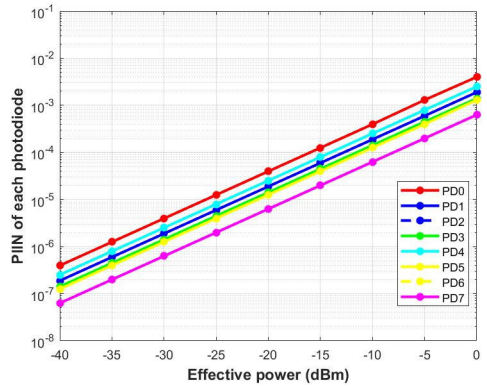

FIGURE 8. PIIN of each PD versus effective received power.

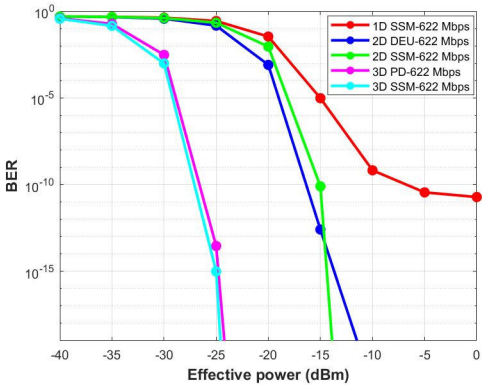

FIGURE 9. BER versus effective received power.

number of users when compared to systems using larger spectral code length. However, practically it requires more number of fibers and star couplers if we increase the value of spatial code length P which increases the complexity of implantation.

Table 4 shows the maximum number of users for 3D-SSM code at BER$\sim$ $\mathbf{10^{-9}}$ at different data rates and different values of spectral and spatial code lengths.

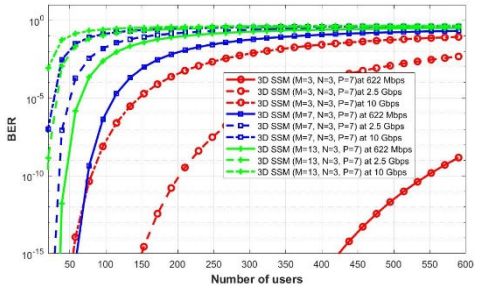

FIGURE 10. BER versus number of users at different spectral code lengths M.

TABLE 4. Maximum number of users for different spectral and spatial code lengths of 3D-SSM code at BER $\sim 10^{-9}$ and various data rates.

Values of M, N, P	Data rate		
	622 Mbps	2.5 Gbps	10 Gbps
3, 3, 7	600	237	97
7, 3, 7	84	36	18
13, 3, 7	48	21	10
3, 3, 13	295	123	59
3, 3, 21	226	96	47

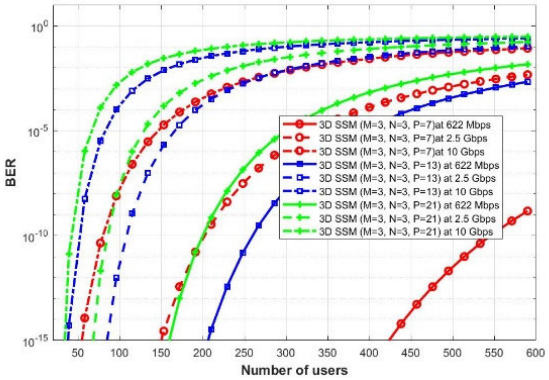

FIGURE 11. BER versus number of users at different spatial code lengths P.

F. SIMULATION RESULTS FOR 3D-SSM CODE AT 5 AND 10 GBPS

As proof of concept, the proposed 3D-SSM code is simulated for different single mode fiber (SMF) lengths at two different data rates using Optisystem software. Table 3 shows the values of the parameters used in simulating the proposed model [18], [21], [22].

The 3D-SSM code sequence implemented in simulation is given in Table 6. This table indicates the encoding (spectral/temporal/spatial) mechanism for 3D-SSM code for eight users.

The 3D SSM code sequences used are implemented as follows:

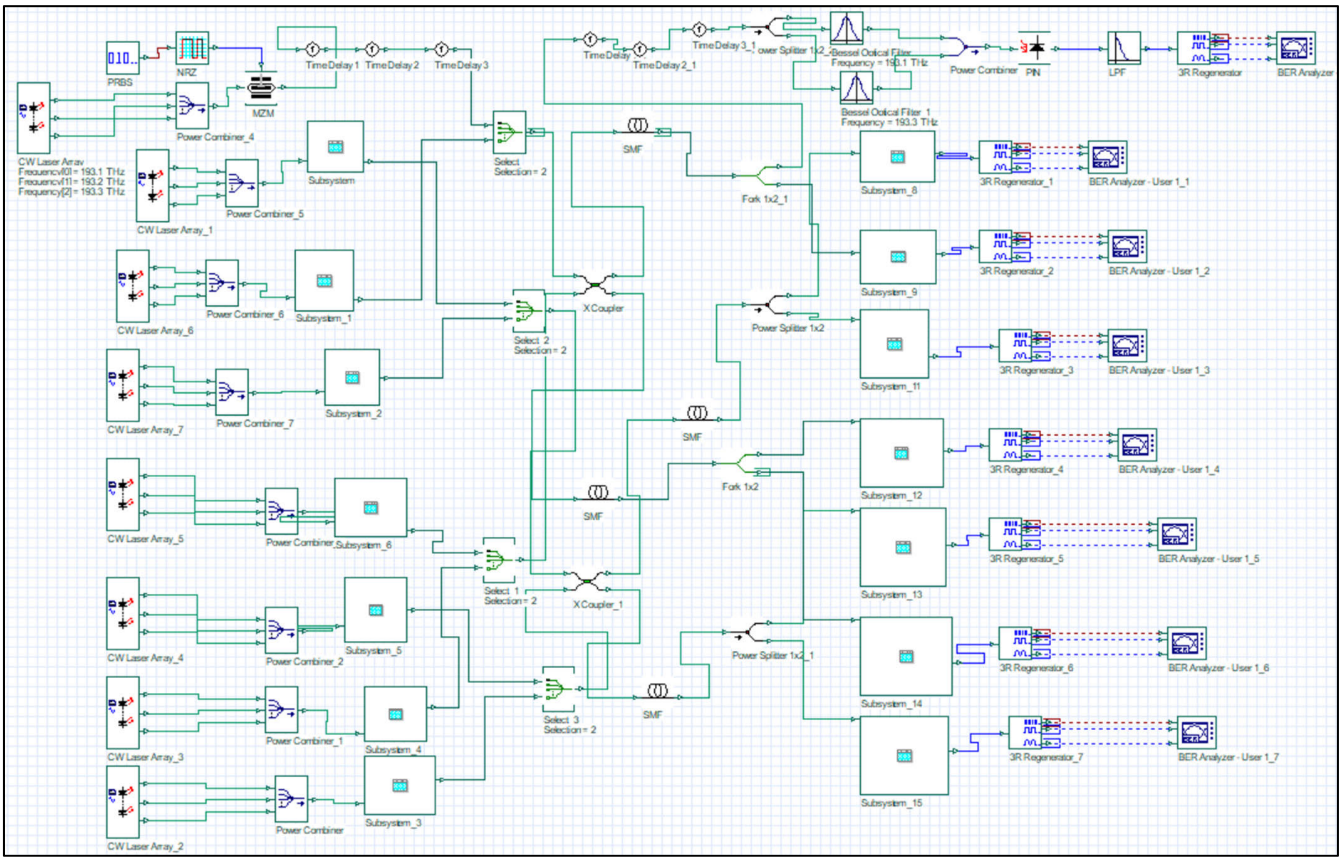

FIGURE 12. Schematic diagram for eight users encoded with 3D SSM code sequence.

TABLE 5. Model parameters values used in simulation.

Parameter	Value (unit)
Data rate (R_b)	5 Gbps, and 10 Gbps
Input source power	10 dBm
Code weight	3
Time delay	0 ns, ($0.25/R_b$) ns, ($0.5/R_b$) ns, ($0.75/R_b$) ns, and ($1/R_b$) ns
Number of users	8
Spectral codelength	3
Temporal code length	3
Spatial code length	3
SMF attenuation	0.25 dB/km
SMF length	From 5 to 20 km
Responsivity of photodetector	0.75 A/W
Dark current	5 nA
Thermal noise	1.38×10^{-23} J/K

- Five laser sources are used to generate five frequencies, which are f_1 =193.1, f_2 =193.2, f_3 =193.3, f_4 =193.4, and f_5 = 193.5 THz. Here, we used two spectral sequences, which are '11100' and '01011', so, for the first code sequence, frequencies f_1, f_2 and f_3 are used, while f_2, f_4, and f_5 are used for the second spectral sequence.
- As the optical bandwidth is divided into five frequencies, so, for time coding, it will be divided into five-time delays, which are t_1 =0, ($t_2 = 0.25\times R_b$), ($t_3 = 0.5\times R_b$), ($t_4 = 0.75\times R_b$), and ($t_5 = 1\times R_b$) ns according to the two temporal code sequences '11100' and '01011'.
- As for spatial coding, five couplers (C1, C2, C3, C4, and C5) are used according to the two spatial code sequences '10011' and '01011'.
- As shown in table 6, user1, user3, user5, and user7 share the same frequencies and time delay and differ in star couplers. Therefore, one code can serve many users by changing either the time delay or star couplers.

Figure 12 shows a schematic diagram for 8 users encoded with 3D SSM code sequences. It consists of laser sources that generate frequencies corresponding to the number of bits '1' present in spectral code sequences. As for the information signal, Pseudo random bit sequence generator (PRBSG) sequence and non-return-to-zero (NRZ) On-OFF keying (OOK) are used. To modulate information signals into optical signals that are generated from laser sources, a Mach-Zehnder modulator (MZM) is used. The output signal

TABLE 6. 3D-SSM code sequences assigned to eight users.

Users	Spectral (THz)					Temporal (×$R_b$ns)					Spatial (coupling)					3D-SSM
	f_1	f_2	f_3	f_4	f_5	t_1	t_2	t_3	t_4	t_5	C1	C2	C3	C4	C5	
1																$f_1f_2f_3t_1t_2t_3C1$
2																$f_2f_4f_5t_2t_4t_5C2$
3																$f_1f_2f_3t_1t_2t_3C4$
4																$f_2f_4f_5t_2t_4t_5C3$
5																$f_1f_2f_3t_1t_2t_3C5$
6																$f_2f_4f_5t_2t_4t_5C4$
7																$f_1f_2f_3t_1t_2t_3C2$
8																$f_2f_4f_5t_2t_4t_5C1$

TABLE 7. BER, Q-factor, and eye diagram at various SMF lengths and 5 Gbps.

Range	BER	Q-factor	Eye diagrams
5 km	1.06×10^{-57}	15.95	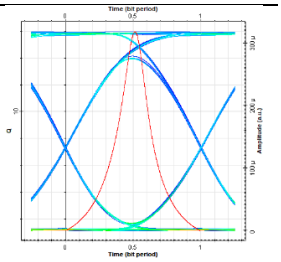
10 km	3.49×10^{-24}	10.04	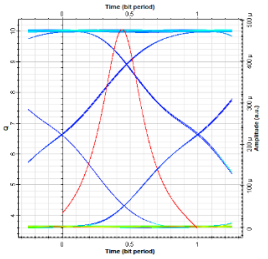
15 km	7.10×10^{-11}	6.38	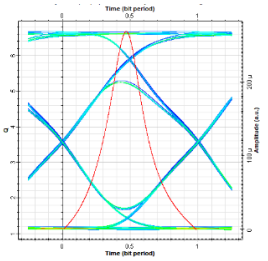
20 km	2.19×10^{-6}	4.43	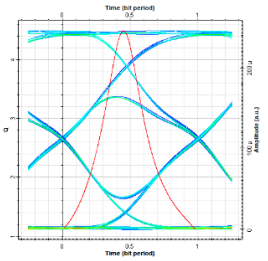

TABLE 8. BER, Q-factor, and eye diagram at various SMF lengths and 10 Gbps.

Range	BER	Q-factor	Eye diagrams
5 km	2.86×10^{-22}	9.60	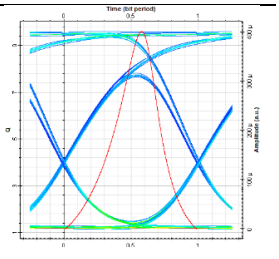
10 km	4.27×10^{-6}	4.40	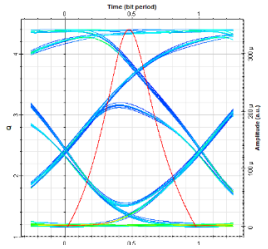
15 km	8.77×10^{-5}	3.71	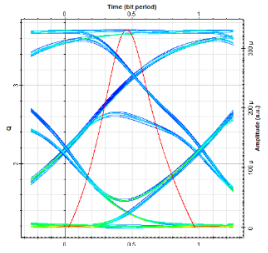
20 km	4.60×10^{-3}	2.55	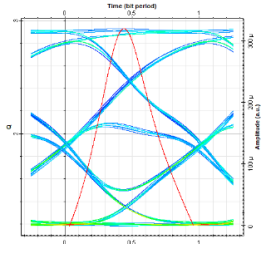

is then delayed according to the temporal code sequence used. Moreover, the resultant optical signal is connected to the coupler for spatial coding, and the signal is encoded with 3D SSM. The signal is then transmitted through SMF until it reaches the receiver side. At the receiver, the signal is split and passed through a delay line so as to be decoded according

to temporal sequence. Furthermore, a decoder using direct detection is used to decode the signal according to spectral sequence, and a photodiode detector is used to convert the signal back to electrical. Finally, a low-pass filter (LPF) and BER analyzer are used, respectively, to reject unwanted signals and test the performance of the received signal.

Tables 6 and 7 show the BER, Q-factor, and eye diagrams for one user for simplicity at different SMF lengths and data rate of 5 Gbps and 10 Gbps, respectively. It is observed that as SMF length increases, the performance degrades. Additionally, the optical signal achieves shorter range when operating at 10 Gbps.

VII. CONCLUSION

In this paper, we have developed an *n*-D algorithm design that generates 1D, 2D and 3D code under OCDMA system. The implementation and performance analysis of a new 3D spectral/temporal/ spatial code for SAC technique is also presented. The code construction and properties of the 3D-SSM, which are extended from the 1D- SSM and 2D-SSM codes are described. In comparison with the system using 2D-SSM codes, the utilization of 3D-SSM codes in the system can effectively reduce the Bit Error Rate (BER) and support a larger number of users. The system performance and simulation results are compared with the published 1D, 2D, and 3D codes for evaluation.

The utilization of 3D-SSM codes has the capability to effectively reduce the impact of PIIN noise, hence resulting in enhanced performance of the system. At received power of -25 dBm, the BERs values for 1D-SSM, 2D-SSM, 2D-DEU, 3D-PD and 3D-SSM codes are 0.2706, 0.2139, 0.1459, $2.909\times\mathbf{10^{-14}}$ and $9.914\times\mathbf{10^{-16}}$, respectively. These findings highlight the flexibility of our system in terms of code dimension, positioning it as a strong candidate for future optical communications.

ACKNOWLEDGMENT

The authors extend their appreciation to Prince Sattam bin Abdulaziz University for funding this research work through the project number (PSAU/2023/01/25208).

REFERENCES

[1] H. Ghafouri-Shiraz and M. M. Karbassian, *Optical CDMA Networks: Principles, Analysis and Applications*. Chichester, U.K.: Wiley, 2012.

[2] A. Cherifi, N. Jellali, M. Najjar, S. A. Aljunid, and B. S. Bouazza, "Development of a novel two-dimensional-SWZCC–code for spectral/spatial optical CDMA system," *Opt. Laser Technol.*, vol. 109, pp. 233–240, Jan. 2019, doi: 10.1016/j.optlastec.2018.07.078.

[3] H. Mrabet, A. Cherifi, T. Raddo, I. Dayoub, and S. Haxha, "A comparative study of asynchronous and synchronous OCDMA systems," *IEEE Syst. J.*, vol. 15, no. 3, pp. 3642–3653, Sep. 2021.

[4] T. B. Osadola, S. K. Idris, I. Glesk, and W. C. Kwong, "Network scaling using OCDMA over OTDM," *IEEE Photon. Technol. Lett.*, vol. 24, no. 5, pp. 395–397, Mar. 1, 2012.

[5] R. Matsumoto, T. Kodama, S. Shimizu, R. Nomura, K. Omichi, N. Wada, and K.-I. Kitayama, "40G-OCDMA-PON system with an asymmetric structure using a single multi-port and sampled SSFBG Encoder/Decoders," *J. Lightw. Technol.*, vol. 32, no. 6, pp. 1132–1143, Mar. 15, 2014.

[6] K. Kitayama, X. Wang, and N. Wada, "OCDMA over WDM PON-solution path to gigabit-symmetric FTTH," *J. Lightw. Technol.*, vol. 24, no. 4, pp. 1654–1662, Apr. 2006.

[7] H. Yin and D. J. Richardson, "Optical code division multiple access communication networks," *Chap*, vol. 1, pp. 36–37, Jan. 2008.

[8] D. Hood and E. Trojer, *Gigabit-Capable Passive Optical Networks: Hood/Optical Networks*. Hoboken, NJ, USA: Wiley, 2012.

[9] K. Meftah, A. Cherifi, A. Dahani, M. Alayedi, and H. Mrabet, "A performance investigation of SAC-OCDMA system based on a spectral efficient 2D cyclic shift code for next generation passive optical network," *Opt. Quantum Electron.*, vol. 53, no. 10, Oct. 2021, doi: 10.1007/s11082-021-03073-w.

[10] S. A. A. El-Mottaleb, H. A. Fayed, N. E. Ismail, M. H. Aly, and M. R. M. Rizk, "MDW and EDW/DDW codes with AND subtraction/single photodiode detection for high performance hybrid SAC-OCDMA/OFDM system," *Opt. Quantum Electron.*, vol. 52, no. 5, pp. 239–259, Apr. 2020.

[11] S. A. A. El-Mottaleb, H. A. Fayed, M. H. Aly, M. R. M. Rizk, and N. E. Ismail, "An efficient SAC-OCDMA system using three different codes with two different detection techniques for maximum allowable users," *Opt. Quantum Electron.*, vol. 51, no. 11, pp. 354–371, Nov. 2019.

[12] S. A. Aljunid, M. Ismail, A. R. Ramli, B. M. Ali, and M. K. Abdullah, "A new family of optical code sequences for spectral-amplitude-coding optical CDMA systems," *IEEE Photon. Technol. Lett.*, vol. 16, no. 10, pp. 2383–2385, Oct. 2004, doi: 10.1109/LPT.2004.833859.

[13] T. Abd, S. Aljunid, H. Fadhil, R. Ahmad, and M. Junita, "Enhancement of performance of a hybrid SAC–OCDMA system using dynamic cyclic shift code," *Ukrainian J. Phys. Opt.*, vol. 13, no. 1, pp. 12–27, 2012, doi: 10.3116/16091833/13/1/12/2012.

[14] H. Y. Ahmed and K. S. Nisar, "Diagonal eigenvalue unity (DEU) code for spectral amplitude coding-optical code division multiple access," *Opt. Fiber Technol.*, vol. 19, no. 4, pp. 335–347, Aug. 2013, doi: 10.1016/j.yofte.2013.04.001.

[15] T. H. Abd, S. A. Aljunid, H. A. Fadhil, R. A. Ahmad, and N. M. Saad, "Development of a new code family based on SAC–OCDMA system with large cardinality for OCDMA network," *Opt. Fiber Technol.*, vol. 17, no. 4, pp. 273–280, Jul. 2011, doi: 10.1016/j.yofte.2011.04.002.

[16] M. Rahmani, A. Cherifi, A. S. Karar, G. Naima Sabri, and B. S. Bouazza, "Contribution of new three-dimensional code based on the VWZCC code extension in eliminating multiple access interference in optical CDMA networks," *Photonics*, vol. 9, no. 5, p. 310, May 2022.

[17] H. Y. Ahmed, M. Zeghid, W. A. Imtiaz, T. Sharma, and A. Chehri, "An efficient 2D encoding/decoding technique for optical communication system based on permutation vectors theory," *Multimedia Syst.*, vol. 27, no. 4, pp. 691–707, Aug. 2021.

[18] T. Sharma, A. Chehri, P. Fortier, H. Yousif Ahmed, M. Zeghid, and W. A. Imtiaz, "Optical code construction of 2D spectral/spatial BIBD codes for SAC–OCDMA systems," *Appl. Sci.*, vol. 11, no. 2, p. 783, Jan. 2021.

[19] H. Yousif Ahmed, M. Zeghid, W. A. Imtiaz, T. Sharma, A. Chehri, and P. Fortier, "Two-dimensional permutation vectors' (PV) code for optical code division multiple access systems," *Entropy*, vol. 22, no. 5, p. 576, May 2020.

[20] H. Y. Ahmed, M. Zeghid, W. A. Imtiaz, and A. Sghaier, "Two dimensional fixed right shift (FRS) code for SAC-OCDMA systems," *Opt. Fiber Technol.*, vol. 47, pp. 73–87, Jan. 2019.

[21] W. A. Imtiaz, H. Y. Ahmed, M. Zeghid, Y. Sharief, and M. Usman, "Design and implementation of two-dimensional enhanced multi-diagonal code for high cardinality OCDMA-PON," *Arabian J. Sci. Eng.*, vol. 44, no. 8, pp. 7067–7084, Aug. 2019.

[22] N. Jellali, M. Najjar, M. Ferchichi, and H. Rezig, "Development of new two-dimensional spectral/spatial code based on dynamic cyclic shift code for OCDMA system," *Opt. Fiber Technol.*, vol. 36, pp. 26–32, Jul. 2017, doi: 10.1016/j.yofte.2017.02.002.

[23] M. Najjar, N. Jellali, M. Ferchichi, and H. Rezig, "Spectral/spatial optical CDMA code based on diagonal eigenvalue unity," *Opt. Fiber Technol.*, vol. 38, pp. 61–69, Nov. 2017, doi: 10.1016/j.yofte.2017.08.003.

[24] R. A. Kadhim, H. A. Fadhil, S. A. Aljunid, and M. S. Razalli, "Performance enhancement of a three dimensional ocdma systems based on a new code," *J. Theor. Appl. Inf. Technol.*, vol. 81, no. 3, p. 589, 2015.

[25] H. Yousif Ahmed, M. Zeghid, W. A. Imtiaz, Y. Sharief, and O. Mohammed Abdalla, "A configurable transmitter-receiver structure to support QoS for spectral amplitude coding-optical code division multiple access," *Opt. Fiber Technol.*, vol. 58, Sep. 2020, Art. no. 102232.

[26] M. Rahmani, A. Cherifi, G. Naima Sabri, M. I. Al-Rayif, I. Dayoub, and B. S. Bouazza, "Performance investigation of 1.5 Tb/s optical hybrid 2D-OCDMA/OFDM system using direct spectral detection based on successive weight encoding algorithm," *Opt. Laser Technol.*, vol. 174, Jul. 2024, Art. no. 110666, doi: 10.1016/j.optlastec.2024.110666.

[27] M. Alayedi, A. Cherifi, A. Ferhat Hamida, and H. Mrabet, "A fair comparison of SAC-OCDMA system configurations based on two dimensional cyclic shift code and spectral direct detection," *Telecommun. Syst.*, vol. 79, no. 2, pp. 193–212, Nov. 2021, doi: 10.1007/s11235-021-00840-8.

[28] N. Jellali, F. Moez, and M. Najjar, "Performance of three dimensional diagonal eigenvalue unity/multi-diagonal code for OCDMA system," in *Proc. Int. Conf. Softw., Telecommun. Comput. Netw. (SoftCOM)*, Sep. 2019, pp. 1–5, doi: 10.23919/SOFTCOM.2019.8903836.

[29] A. Cherifi, T. Mohammed Chikouche, A. S. Karar, J. M. H. Barakat, O. Arbouche, and I. Dayoub, "Capacity improvement of 3D-OCDMA-PON hybrid system next generation using weight zero cross correlation code," *Appl. Sci.*, vol. 13, no. 10, p. 5869, May 2023, doi: 10.3390/app13105869.

HASSAN YOUSIF AHMED received the B.Eng. degree in computer engineering (network systems) and the M.Sc. degree in computer science and information from Gezira University, Sudan, in 2002 and 2007, respectively, and the Ph.D. degree in electrical and electronic engineering from Universiti Teknologi PETRONAS, Malaysia, in 2010. He is currently a Full Professor with the Electrical Engineering Department, College of Engineering, Prince Sattam Bin Abdulaziz University. His research interests include computer networks, wireless communications networks, optical communications, and cryptography systems.

MEDIEN ZEGHID received the Ph.D. degree in information and communication, sciences and technologies from the University of Southern Brittany, Lorient, France, in 2011. He was an Assistant Professor with the Department of Electronic Engineering, Higher Institute of Applied Sciences and Technology of Sousse, Sousse University, Tunisia, from 2012 to 2014. He is currently an Assistant Professor with the Department of Computer Engineering and Networks, Prince Sattam Bin Abdulaziz University. His research interests include information security, architectural synthesis for crypto-systems, image and video coding, and optical communication.

MAISARA MOHYELDIN GASIM received the B.S. and M.S. degrees in mechanical engineering from the University of Khartoum, Khartoum, Sudan, in 1996 and 2001, respectively, and the Ph.D. degree from Sudan University of Science and Technology, in 2007. He is currently an Assistant Professor with the Mechanical Engineering Department, College of Engineering, Prince Sattam Bin Abdulaziz University. His research interests include mobile applications, modern internal combustion engines, and the Internet of Things.

SOMIA A. ABD EL-MOTTALEB received the B.Sc. degree in electrical (electronics and communications) engineering from the Faculty of Engineering, Alexandria University, in 2010, the M.Sc. degree in electronics and communications engineering from the Faculty of Engineering, Arab Academy for Science, Technology and Maritime Transport, in 2014, and the Ph.D. degree in electrical (electronics and communications) engineering from the Faculty of Engineering, Alexandria University, in 2020, with a focus on optical communication. She is currently a Lecturer with Alexandria Higher Institute of Engineering and Technology, Alexandria, Egypt. She has published papers in Q1 and Q2 Scopus journals. Her research interests include free space optics, optical amplifiers, detection techniques, multiplexing techniques, optical fiber communications, and the Internet of Things.